Efficient Directional Excitation of Surface Plasmons by a Single-Element Nanoantenna

Wenjie Yao,[§,†] Shang Liu,[§,†] Huimin Liao,[*,†] Zhi Li,[*,†] Chengwei Sun,[†,‡] Jianjun Chen,[†,‡] and Qihuang Gong[†,‡]

[†]School of Physics, Peking University, Beijing 100871, China

[‡]State Key Laboratory for Mesoscopic Physics, Peking University, Beijing 100871, China

Ⓢ *Supporting Information*

ABSTRACT: Directional light scattering is important in basic research and real applications. This area has been successfully downscaled to wavelength and subwavelength scales with the development of optical antennas, especially single-element nanoantennas. Here, by adding an auxiliary resonant structure to a single-element plasmonic nanoantenna, we show that the highly efficient lowest-order antenna mode can be effectively transferred into inactive higher-order modes. On the basis of this mode conversion, scattered optical fields can be well manipulated by utilizing the interference between different antenna modes. Both broadband directional excitation of surface plasmon polaritons (SPPs) and inversion of SPP launching direction at different wavelengths are experimentally demonstrated as typical examples. The proposed strategy based on mode conversion and mode interference provides new opportunities for the design of nanoscale optical devices, especially directional nanoantennas.

KEYWORDS: nanoantenna, surface plasmon polaritons, directional scattering, mode conversion, single-element
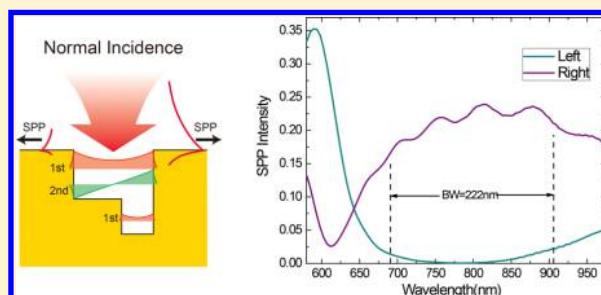
Light field manipulation is a basic subject in optics and has several important applications. With the development of nano-optics, this area has been downscaled to nanoscales accompanied by several important progresses.[1−3] Typical nanoscale devices, such as nanowaveguides,[4] nanoantennas,[5−7] and nanolasers[8,9] have been proposed and demonstrated. Among these devices, nanoantennas are important because of their ability to control the absorption and radiation of light at nanoscale dimensions. Especially, proper designs of nano-antennas provide efficient means to control the directionality of scattered optical fields.[6,7] This phenomenon is highly desired in many applications, including communications, solar cells, and sensors, among others.

Optical nanoantennas could be analogously designed with classical microwave antennas to achieve directional light scattering. By carefully regulating the scattering amplitudes, phases, and spatial separations of a series of antenna elements, multielement antennas, such as the Yagi−Uda configuration,[6,7] have been proposed to control absorption and emission directions based on constructive and destructive interferences in different directions. However, these multielement antennas are relatively large in size and complex to fabricate. To overcome these deficiencies, single-element nanoantennas have been proposed to obtain strong directional scattering.[10−14] Instead of using the interference between different antenna elements in a multielement antenna, a single-element nano-antenna utilizes interference between different optical modes of an antenna. Unfortunately, higher-order optical modes

generally cannot be excited as efficiently as the lowest mode by external optical fields because strong field gradients on the nanoscales are required to match the complex modal fields of higher-order modes. Consequently, structures of either single-element antennas[12,13] or external excitation fields[14] must be well designed and controlled; thus, increased complexities in sample fabrications or experiments are expected.

In this study, we explore a novel degree of freedom to effectively excite higher-order antenna modes, which is through mode conversion. Mode conversion has been utilized to excite dark modes in plasmonic structures.[15,16] However, the conversion efficiencies are generally quite limited because the conversions are conducted by nonresonant structures. Here, by adding an auxiliary resonant structure to the main structure of a single-element nanoantenna, we show that the energy of the highly efficient lowest-order antenna mode can be effectively transferred into higher-order modes with the aid of the participation of the optical mode in the auxiliary structure. This phenomenon greatly facilitates further manipulations of scattered optical fields by exploiting the interference between different antenna modes. As a proof of principle, we demonstrate a single-element nanoantenna for efficient directional excitation of surface plasmon polaritons (SPPs)[17−24] by
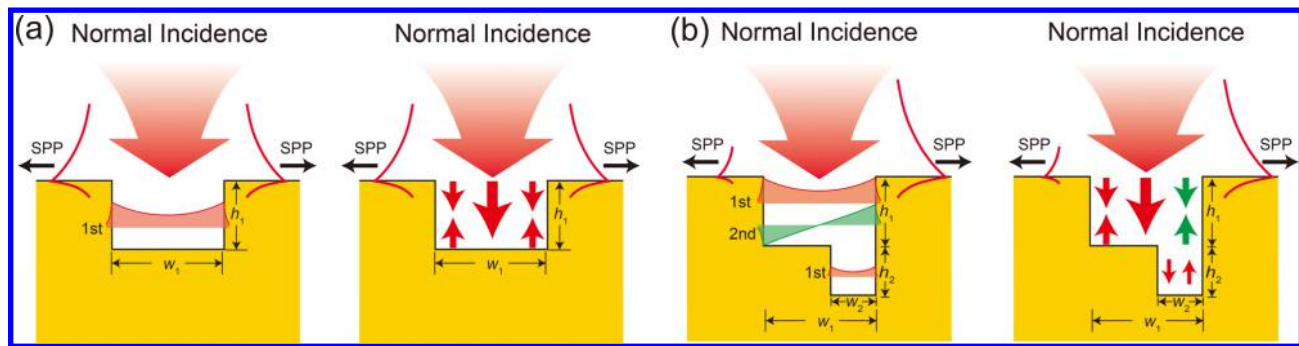
Figure 1. Schematic diagrams of SPP excitations by a single-element plasmonic nanoantenna without and with an auxiliary structure. The left panels in (a) and (b) show the modal field distributions of different waveguide modes in the metallic grooves, whereas the right panels indicate corresponding mode propagating processes (red and green arrows represent the first and second modes, respectively). (a) At normal incidence, only the symmetric first mode in the subwavelength groove without an auxiliary structure can be excited because of excitation symmetry. This causes equal SPP launching intensities to the left and right directions. (b) The energy of the active first mode in the main groove can be effectively transferred into the energy of the inactive second mode when a small auxiliary nanogroove is added to the bottom of the main groove. This phenomenon enables the antenna to further manipulate scattered optical fields (for instance, to obtain directional SPP excitation) through the interference between the symmetric first and antisymmetric second modes.

utilizing the mode conversion between an active first-order and inactive second-order mode in a subwavelength metallic groove. Inversion of SPP launching direction at different wavelengths is also observed, which is attributed to the contribution of a nonpropagating (i.e., below cut off) third-order mode. The proposed method based on mode conversion and mode interference provides new opportunities for the design of nanoscale optical devices, especially in the research area of directional nanoantennas.

The sample structure considered in this study is a subwavelength groove on a metal surface, which could be regarded as an efficient plasmonic antenna.[25,26] SPPs can be launched with high efficiency when the structure is illuminated by a normal incident beam. However, only the symmetric first-order (first) waveguide mode in the subwavelength metallic groove is active because of excitation symmetry in normal incidence. This feature causes equal SPP launching intensities to the left and right directions, as schematically shown in Figure 1a. To obtain directional SPP excitation, the antisymmetric second-order (second) waveguide mode in the groove must become active (for detailed information concerning different waveguide modes in the metallic grooves, see Section 1 in the Supporting Information). Although this occurrence can be achieved via oblique incidence,[27,28] low absolute efficiency becomes a drawback because an excitation beam cannot be tightly focused in oblique incidence. This study explores a novel degree of freedom to efficiently excite the antisymmetric second mode through mode conversion. This is realized by adding a small auxiliary nanogroove to the bottom of the main groove, as schematically shown in Figure 1b. The symmetric first waveguide mode in the main groove is excited with high efficiency when a normal incident beam is tightly focused to the entrance of the upper main groove. This waveguide mode propagates downward and excites the first waveguide mode in the lower auxiliary nanogroove which then gets highly reflected at the metallic groove bottom. The first waveguide mode in the auxiliary nanogroove exhibits strong field gradients on the nanoscale and partly overlaps with the antisymmetric second mode in the main groove (see the left figure in Figure 1b). Therefore, the reflected first mode in the auxiliary nanogroove can effectively excite and activate the second mode in the upper main groove; consequently, the energy of the active first mode

in the main groove can be successfully converted into the energy of the inactive second mode, with the aid of the auxiliary structure. This phenomenon enables the antenna to further manipulate scattered optical fields (for instance, to obtain directional SPP excitation) through the interference between the symmetric first and antisymmetric second modes. The above mechanism of mode conversion and mode interference can be theoretically described by a semianalytical model, which is provided in detail in Section 2 in the Supporting Information, and calculation results by this model quantitatively agree with the direct simulation results. It is also noted that, although the proposed antenna structure in Figure 1b looks similar to the previously reported asymmetric slit structures (e.g., in Reference 18), the underlying physical mechanism is completely different (for detailed comparison between the two structures, see Section 3 in the Supporting Information).

We perform numerical simulations using finite element method (FEM) by COMSOL Multiphysics to verify the above idea of mode conversion. The permittivity of gold as a function of wavelength is taken from a previous literature,[29] and the value is expanded using the method of interpolation. The incident wavelength is initially set to $\lambda = 800$ nm. For simplicity, the width of the auxiliary nanogroove is fixed to $w_2 = 200$ nm ($\sim 0.25\lambda$) so that only the first waveguide mode exists in the auxiliary nanogroove. The width of the main groove is set to $w_1 = 550$ nm ($\sim 0.7\lambda$), which ensures that only the first and second waveguide modes are propagating modes in the main groove. When downward propagating, the first or second waveguide mode in the upper main groove encounters the lower auxiliary nanogroove, they are partly reflected and partly transferred into each other (see the right-side inset in Figure 2). The mode-conversion behavior can be quantitatively described by a reflection matrix **R**, with the matrix element R_{ij} ($i,j = 1,2$) denoting the conversion coefficient from the downward jth mode to the upward ith mode and $|R_{ij}|^2$ representing the power flow of the upward ith mode when the incident power flow of the downward jth mode is normalized to be unity at the bottom of the main groove. Figure 2 shows the calculated amplitudes of the four matrix elements ($|R_{ij}|$) at various depths h_2 of the auxiliary nanogroove. These coefficients are extracted from the total electromagnetic field by using mode orthogonality between different waveguide modes in waveguide theories.[30,31]
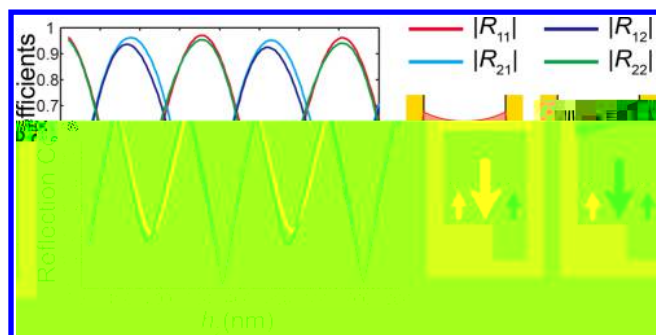
Figure 2. Efficient mode conversion in a single-element plasmonic nanoantenna with the auxiliary structure. The left panel shows calculated amplitudes of the four elements of the reflection matrix **R** at various depths h_2 of the auxiliary nanogroove (incident wavelength λ = 800 nm, groove widths w_1 = 550 nm and w_2 = 200 nm). The right-side inset provides a schematic explanation to the four matrix elements.

The cross-conversion coefficients between the two modes ($|R_{12}|$ and $|R_{21}|$) vary from 0 to 0.95, which can be well controlled through h_2. This means that up to 90% of the power of incident mode can be transferred into the power of the other mode. Therefore, mode conversion provides a highly efficient means of exciting the inactive second mode in the single-element antenna, considering that the symmetric first mode can be excited by normal incident beam with very high efficiency.[25,26] Meanwhile, this method exhibits the advantage of having no critical requirement on external excitation fields and only weakly increases the complexity of sample fabrication.

Because higher-order antenna modes in a single-element nanoantenna can be effectively excited through mode conversion, further manipulation of scattered optical fields becomes convenient. For instance, we demonstrate directional excitation of SPPs,[17−24] which is highly desired in many plasmonic applications. Figure 3a schematically shows the three main origins of the final SPPs on the front metal surface excited by the proposed antenna structure in Figure 1b. These origins include the SPPs excited by the directly incident beam and the upward propagating first and second modes at the entrance of the upper main groove. The SPPs launched to the left and right directions are in phase for the first two origins (indicated by two cross-in-circle symbols on the left and right sides), but in antiphase in the antisymmetric second mode excitation (indicated by a dot in circle symbol on the left side and a cross in circle on the right side). This implies that the three SPP components may just cancel each other in one direction and interfere constructively in the other direction under proper conditions. Thus, a highly efficient directional excitation of SPPs is obtained.

The specific condition can be achieved by adjusting the depths h_1 and h_2 of the main and auxiliary grooves because amplitudes of the upward first and second modes can be primarily controlled by h_2 through mode conversion, whereas the phase difference between the two modes can be adjusted by h_1. Figure 3b shows the simulated SPP intensities (quantified by SPP power flows normalized by the incident power flow on the groove entrance) that are launched to the left and right directions at various h_1 and h_2. Each peak of the leftward SPP intensity approximately corresponds to a trough in the rightward SPPs, and vice versa. Thus, by choosing proper groove depths, highly directional SPP excitations can be achieved in both the left and right directions (for details, see Figures S10 and S11 in the Supporting Information). For comparison, the previously reported asymmetric slits enable
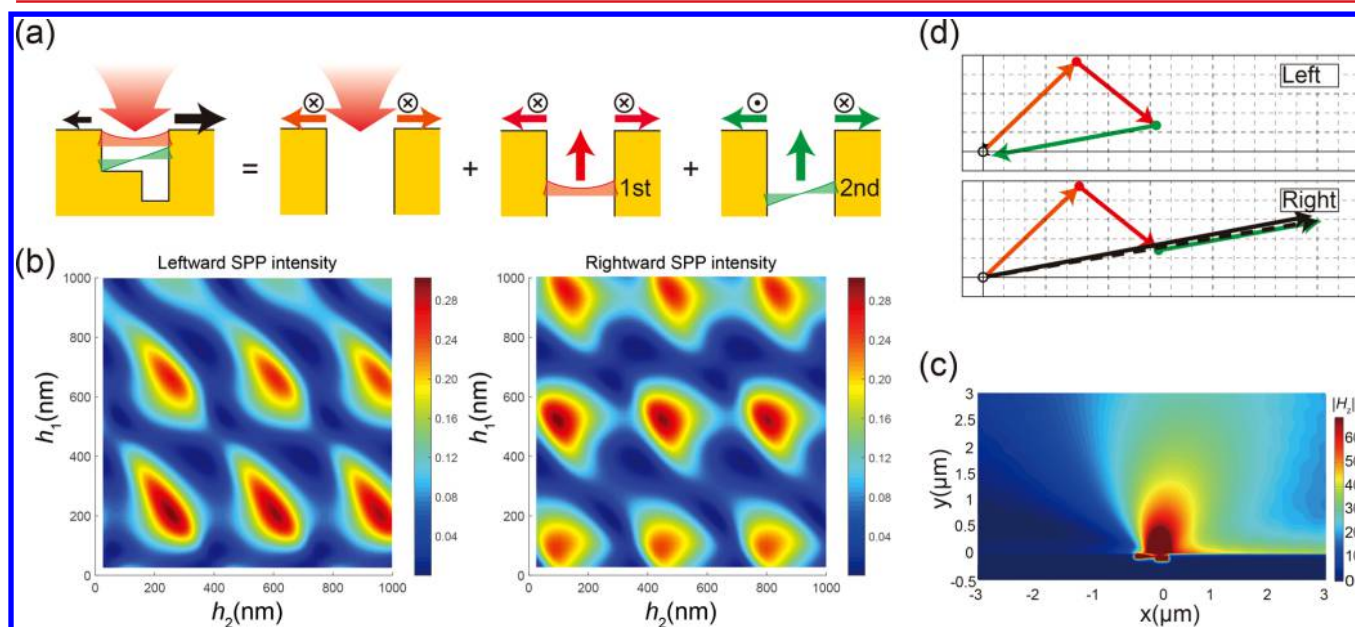
Figure 3. Directional excitation of SPPs by a single-element plasmonic nanoantenna with an auxiliary structure. (a) Three main origins of final SPPs on the front metal surface. These origins include SPPs excited at the entrance of the upper main groove by directly incident beam and upward propagating first and second modes. The cross in circle and dot in circle symbols represent the magnetic field is directed into and out of the plane of the figure, respectively. These symbols are engage to indicate the symmetry of different modes. (b) SPP intensities launched to the left and right directions by the proposed antenna structure in Figure 1b, at various h_1 and h_2. (c) Simulated magnitude of scattered magnetic field under a specific geometry of h_1 = 79 nm and h_2 = 52 nm, with unidirectional launching of SPPs to the right clearly observed. (d) Corresponding vector diagrams displaying the three main SPP contributions to total SPPs. The meaning of each color vector is indicated on the front metal surface in panel a. All above calculations are performed at λ = 800 nm, w_1 = 550 nm, and w_2 = 200 nm.
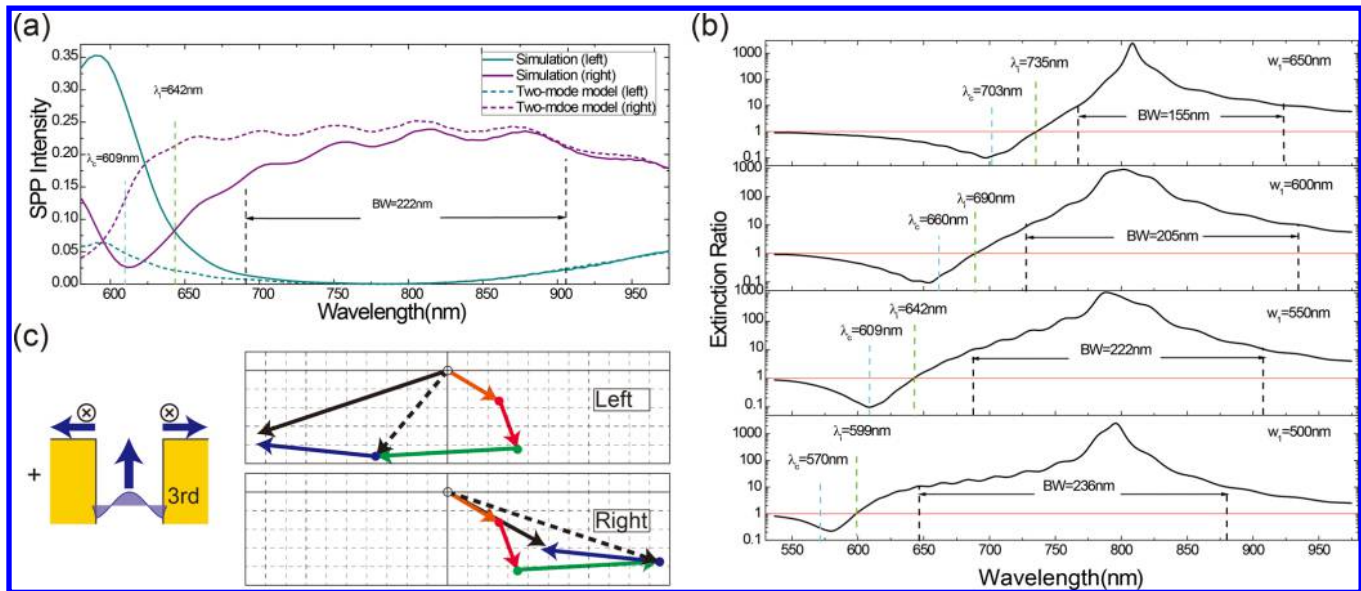
Figure 4. Wavelength response of directional SPP excitations by the proposed single-element plasmonic nanoantenna. (a) Simulated total SPP intensities (solid lines) to the left and right directions at various incident wavelengths and corresponding two-mode model results (dashed lines) that only take into account the SPP contributions from the directly incident beam and first and second modes in the main groove. (b) Simulated E_R spectra at w_1 = 500, 550, 600, and 650 nm. w_2 is fixed at 200 nm and h_1 and h_2 are adjusted to achieve the highest E_R at λ = 800 nm. The dashed lines indicate the critical wavelength λ_i at which E_R = 1 and the cutoff wavelength λ_c of the third mode in the main groove. (c) Vector diagrams showing different SPP contributions at λ = 626 nm. In addition to the three SPP contributions at λ = 800 nm in Figure 3d, the SPPs excited by the nonpropagating (or evanescent) third mode, which are represented by the blue vectors, play a significant role. The left inset provides a schematic explanation of this SPP component.

unidirectional SPP excitation to only one direction.[18] In real experiments, small groove depths are preferred because they are easy to fabricate. Therefore, the smallest possible groove depths of h_1 = 79 nm and h_2 = 52 nm are chosen in this study. Figure 3c shows the corresponding scattered field by the proposed single-element nanoantenna. A nearly perfect directional launching of SPPs to the right is clearly observed. The extinction ratio E_R, which is defined as the rightward SPP intensity over the leftward one, is >10³. The specific contributions of the three main SPP origins were evaluated by calculating the three basic SPP excitation processes on the right side of the "=" in Figure 3a one by one. The results are intuitively indicated by vectors in Figure 3d with the vector lengths and directions corresponding to the amplitudes and phases of different SPP components (for more detailed information on the vector diagram, see Section 4 in the Supporting Information). The orange and red vectors, respectively, correspond to the SPPs excited by the directly incident beam and the upward symmetric first mode. Figure 3d shows that both these two SPP contributions are in phase for the left and right directions. On the contrary, the SPPs excited by the antisymmetric second mode are in antiphase for the left and right directions. Thus, these antiphase SPPs are represented by two opposite green vectors in Figure 3d, one vector denoting the left and the other denoting the right. The green vector denoting the left just cancels the summation of the orange and red vectors. This results in SPP extinction in this direction. Meanwhile, the opposite green vector denoting the right constructively interferes with the summation of the orange and red vectors. This occurrence causes highly efficient directional SPP launching to the right direction. The total SPPs on the front metal surface are also directly evaluated and indicated by the black solid vectors in Figure 3d. These vectors agree well with the summation of the three color vectors which

are indicated by the black dashed vectors. In the figure, black vectors representing the left direction are extremely short to be seen because of the SPP extinction. Thus, the previous model analysis and proposal for directional SPP excitation are well confirmed, and the key role of effective excitation of the antisymmetric second mode is clearly presented. Further simulations show that up to 21% of the total incident power can be launched into the rightward SPPs for a tightly focused Gaussian incidence with a waist size of w_0 = 480 nm. This absolute coupling efficiency is rather high, considering the subwavelength lateral dimension of the proposed antenna structure. For comparison, the efficiency of the antenna without an auxiliary nanogroove reaches only 11%.

The above results are obtained with specific geometrical parameters of w_1 = 550 nm and w_2 = 200 nm. More simulations show that the main conclusions (i.e., efficient mode conversion and directional SPP excitation) can be extended to more general cases as long as the main groove supports only the first and second modes and the auxiliary nanogroove supports only the first mode.

Wavelength-dependent property is an important aspect for a directional nanoantenna. The cyan and purple solid lines in Figure 4a show simulated SPP intensities to the left and right directions at various incident wavelengths (with w_1 = 550 nm, w_2 = 200 nm, h_1 = 79 nm, and h_2 = 52 nm). Directional SPP excitation clearly presents a broadband response around the central wavelength of λ = 800 nm. The third panel in Figure 4b shows the corresponding spectrum of the extinction ratio E_R. Here, we define the bandwidth (BW) of a directional SPP excitation as the wavelength range over which $E_R \geq 10$, considering that such an E_R value is sufficient for enormous unidirectional SPP couplers. For the current case, BW reaches 222 nm, which is a fairly satisfactory outcome. This broadband response is mainly attributed to the shallow grooves used in the
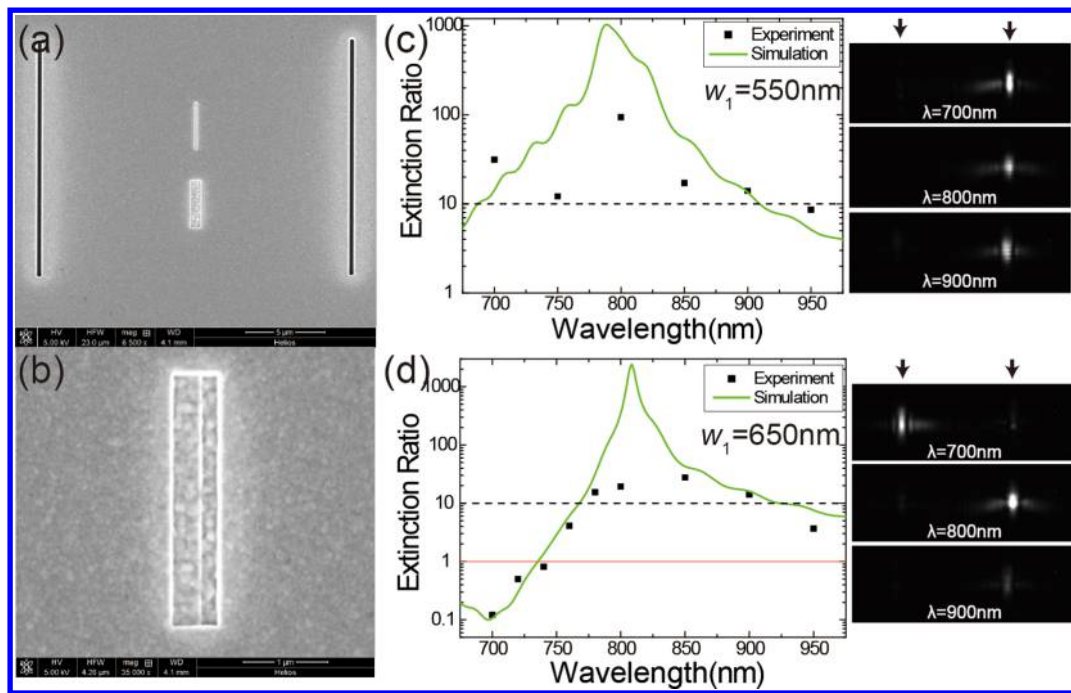
Figure 5. Experimental verification of directional SPP excitations using the proposed plasmonic nanoantenna. (a) SEM image of the structure of a sample. In the middle of the image, the proposed single-element nanoantenna is at the lower half, and a simple 100-nm-wide nanogroove at the upper half acts as an in-chip reference. Two observation slits that cut through the metal film and lie symmetrically on two sides of the central structure with a distance of 10 μm are designed to reconvert launched SPPs back into photons. (b) SEM image that shows a closer look of the proposed single-element nanoantenna with an auxiliary nanogroove. (c) Extinction ratio E_R at different wavelengths for sample 1 (w_1 = 550 nm, h_1 = 79 nm, w_2 = 200 nm, and h_2 = 52 nm), which presents the best broadband response of SPP directional excitation. (d) Extinction ratio E_R at different wavelengths for sample 2 (w_1 = 650 nm, h_1 = 87 nm, w_2 = 200 nm, and h_2 = 33 nm), which shows direction inversion of SPP excitation. The scatters are experimental results, and the green lines are simulation results. The right-side insets show typical CCD images, wherein directional SPP excitations are clearly observed (arrows indicate the locations of the two observation slits).

study. Small groove depths mean slow variations in the propagating phase factors of different modes when incident wavelength changes. Therefore, the resulting bandwidth is large. In contrast, BW decreases to 50 nm if another optimized geometry with deeper grooves of h_1 = 550 nm and h_2 = 440 nm are selected for achieving directional SPP excitation at λ = 800 nm.

Another interesting feature is the inversion of SPP launching direction at different wavelengths. In contrast to the slow variations in SPP intensities near the central wavelength of λ = 800 nm, SPP intensities change rapidly at the short-wavelength region, and the leftward SPP intensity rapidly exceeds the rightward intensity. A minimum E_R of 0.1 is obtained at λ = 609 nm. This value means that a highly directional SPP excitation to the left direction is achieved. Several E_R spectra at different w_1 are calculated to understand the underlying physical mechanism of SPP direction inversion. In the simulations, w_2 is fixed at 200 nm and h_1 and h_2 are adjusted to achieve the highest E_R at the same central wavelength of λ = 800 nm. The results are shown in different panels in Figure 4b. E_R remains high over a wide wavelength range near λ = 800 nm in all the four panels, which indicates that broadband directional SPP excitations to the right direction occur. Meanwhile, all of the SPP excitation directions change to the left direction at short wavelengths. The inversion wavelength λ_i, which is defined as the critical wavelength at which E_R = 1, increases with w_1. This phenomenon implies that the third-order (third) mode in the main groove may play a role because the cutoff wavelength λ_c of this mode also increases with w_1 (for the definition and evaluation of λ_c, see Section 1 in the Supporting Information). The dashed lines in

Figure 4b indicate the locations of λ_i and λ_c. Although λ_i and λ_c do not coincide with each other, a clear correlation is observed. To test the above hypothesis, we introduce the two-mode model that calculates the summation of SPP components contributed by the directly incident beam, first and second modes (for detailed information on the two-mode model, see Section 4 in the Supporting Information). Therefore, the discrepancy between the results of this model and the direct simulation results that naturally include SPP components contributed by all waveguide modes can intuitively indicate the SPP contributions from nonpropagating modes. The cyan and purple dashed lines in Figure 4a show the results of this model, which agree with direct simulation results in the long-wavelength region but deviates more and more toward the cutoff wavelength λ_c of the third mode. This phenomenon directly reflects the impact of the third mode. As a typical example, the vector diagrams in Figure 4c show the different SPP components at λ = 626 nm (i.e., in the middle of λ_i and λ_c). Contrary to the results at λ = 800 nm which are shown in Figure 3d, summations of the orange, red, and green vectors (i.e., results of the two-mode mode), which are indicated by the black dashed vectors, now significantly deviate from the actual total SPPs (black solid vectors). Only when the SPP contributions from the third mode are taken into account, the modified-model results can match the direct simulation results. The SPP contributions from the third mode are represented by the two blue vectors in Figure 4c. These two vectors point to the same direction because the third mode is a symmetric mode. The above results clearly validate the previous hypothesis on the role of the third mode at the short-

wavelength region. The total SPPs change the launching direction because of the SPP contribution of this high-order mode. Without the contribution of this mode, the previous two-mode model still gives a directional SPP excitation to the right direction.

One thing needs special attention is that λ_i is obviously larger than λ_c. This means that the third mode starts to play a significant role even when it is nonpropagating (namely, below cut off) or evanescent. The reason is that the groove is so shallow that even the exponentially decaying nonpropagating mode maintains a considerable intensity over such a subwavelength distance. That is why the SPPs contributed by the nonpropagating third mode are comparable to or even stronger than the SPPs contributed by the propagating second and first modes at $\lambda = 626$ nm, as shown in Figure 4c. The observed inversion of SPP launching direction indicates that the exploitation of nonpropagating modes may provide new possibilities to the design of nanoscale optical devices in addition to conventional propagating modes. However, this strategy is only applicable when the nonpropagating mode is not far below the cut off. Otherwise, the SPP contribution by this mode is negligible because of the significant propagation loss. That is why the third mode need not to be considered at $\lambda = 800$ nm, which is much larger than $\lambda_c = 609$ nm.

To validate our proposal experimentally, the sample structures were fabricated using direct focused ion beam (FIB) milling on a 450-nm-thick gold film that was evaporated on a glass substrate. Figure 5a shows a typical scanning electron microscope (SEM) image. Two 3-μm-long grooves are presented in the middle of the image. The lower groove is the proposed single-element plasmonic nanoantenna with an auxiliary nanogroove. Figure 5b provides a detailed image of this antenna. The upper groove is a simple 100-nm-wide nanogroove, which acts as an in-chip reference for sample alignment. Two nanoslits that cut through the metal film and lie symmetrically on the two sides of the central structure are designed to reconvert the launched SPPs back into photons. Thus, far-field detected signals provide a direct measurement of the relative intensities of evanescent SPPs.

The laser source is a Ti:sapphire laser, and its wavelength is tunable from 700 to 950 nm. In the measurement, the nanoantenna was normally illuminated from the front side using a p-polarized (electric field perpendicular to the groove) laser beam with a diameter of approximately 3 μm. A fraction of the launched SPPs that leak through the observation slits was collected using an objective from the substrate side and imaged onto a charge coupled device (CCD). Thus, the extinction ratio of the proposed antenna structure could be measured by comparing the signal intensities of the two observation slits. These signal intensities are evaluated by integrating over the detected light spots. The scatters in Figure 5c and d show the measured results at different incident wavelengths. Figure 5c displays the results obtained from sample 1 ($w_1 = 550$ nm, $h_1 = 79$ nm, $w_2 = 200$ nm, and $h_2 = 52$ nm). This sample is chosen to present the best broadband response of SPP directional excitation in the measured spectral range from 700 to 950 nm. The observed bandwidth that exhibits an $E_R \geq 10$ is larger than 200 nm. The insets in Figure 5c demonstrate the typical CCD images taken at $\lambda = 700$, 800, and 900 nm. These images clearly show the high contrast between the SPPs launched to the left and right directions. The measured maximum E_R reaches 94 at $\lambda = 800$ nm. Figure 5d displays the results obtained from sample 2 ($w_1 = 650$ nm, $h_1 = 87$ nm, $w_2 = 200$

nm, and $h_2 = 33$ nm). This sample is selected to demonstrate the direction inversion of SPP excitation. The insets in Figure 5d show that the SPPs are primarily launched to the left direction at $\lambda = 700$ nm (left:right = 8:1) and the right direction at $\lambda = 800$ nm (left:right = 1:19). Direction inversion of SPP excitation is clearly observed. The measured spectra of E_R for both two samples consist with FEM simulation results (lines in Figure 5c and d). Only extinction ratios with extremely high values are not as high as the simulation results. This is understandable considering that the samples are not perfectly fabricated, and roughness of the sample decreases device performance. This deficiency may be overcome by using other fabrication techniques which provide decreased sample roughness, such as template stripping methods.[32] Nevertheless, the measured high extinction ratio itself has already validated the theoretical prediction of directional SPP excitation.

In conclusion, this study demonstrates that highly efficient lowest-order mode can be effectively transferred into higher-order modes by adding an auxiliary resonant structure to the main structure of a single-element plasmonic nanoantenna. This mode conversion provides a novel degree of freedom to effectively excite higher-order antenna modes, which greatly facilitates further manipulations of scattered optical fields. As typical examples, both broadband directional excitation of SPPs and inversion of SPP launching direction at different wavelengths are presented, which are unable to be obtained simultaneously in any previously reported structures. Although the current work is performed under the specific configuration of metallic groove antenna, the strategy of exploiting mode conversion and mode interference can be applied to various antenna structures, such as metallic nanostripe antennas, metallic slot antennas, metallic nanorod antennas, or even dielectric nanoantennas. Therefore, the proposed method based on mode conversion and mode interference provides new opportunities for the design of nanoscale optical devices, especially in the research area of directional nanoantennas.

■ ASSOCIATED CONTENT

Ⓢ Supporting Information

Information on different waveguide modes, a semianalytical model describing the mode conversion and interference processes, comparison between the asymmetric slit and groove structures, and details on vector diagrams and the two-mode model. This material is available free of charge via the Internet at http://pubs.acs.org.

■ AUTHOR INFORMATION

Corresponding Authors
*E-mail: HMLiao@pku.edu.cn
*E-mail: z_li@pku.edu.cn.

Author Contributions
§W. Y. and S. L. contributed equally to the work.

Notes
The authors declare no competing financial interest.

■ ACKNOWLEDGMENTS

■ REFERENCES

(1) Lal, S.; Link, S.; Halas, N. J. *Nat. Photonics* **2007**, *1*, 641−648.

(2) *Nano-Optics and Near-Field Optical Microscopy*; Zayats, A. V., Richards, D., Eds.; Artech House: Boston, 2009.

(3) Schuller, J. A.; Barnard, E. S.; Cai, W. S.; Jun, Y. C.; White, J. S.; Brongersma, M. L. *Nat. Mater.* **2010**, *9*, 193−204.

(4) Bozhevolnyi, S. I.; Volkov, V. S.; Devaux, E.; Laluet, J.-Y.; Ebbesen, T. W. *Nature* **2006**, *440*, 508−511.

(5) Mühlschlegel, P.; Eisler, H.-J.; Martin, O. J. F.; Hecht, B.; Pohl, D. W. *Science* **2005**, *308*, 1607−1609.

(6) Kosako, T.; Kadoya, Y.; Hofmann, H. F. *Nat. Photon* **2010**, *4*, 312−315.

(7) Curto, A. G.; Volpe, G.; Taminiau, T. H.; Kreuzer, M. P.; Quidant, R.; van Hulst, N. F. *Science* **2010**, *329*, 930−933.

(8) Noginov, M. A.; Zhu, G.; Belgrave, A. M.; Bakker, R.; Shalaev, V. M.; Narimanov, E. E.; Stout, S.; Herz, E.; Suteewong, T.; Wiesner, U. *Nature* **2009**, *460*, 1110−1112.

(9) Oulton, R. F.; Sorger, V. J.; Zentgraf, T.; Ma, R. M.; Gladden, C.; Dai, L.; Bartal, G.; Zhang, X. *Nature* **2009**, *461*, 629−632.

(10) Rolly, B.; Stout, B.; Bonod, N. *Opt. Express* **2012**, *20*, 20376−20386.

(11) Fu, Y. H.; Kuznetsov, A. I.; Miroshnichenko, A. E.; Yu, Y. F.; Luk'yanchuk, B. *Nat. Commun.* **2013**, *4*, 1527.

(12) Vercruysse, D.; Sonnefraud, Y.; Verellen, N.; Fuchs, F. B.; Di Martino, G.; Lagae, L.; Moshchalkov, V. V.; Maier, S. A.; Van Dorpe, P. *Nano Lett.* **2013**, *13*, 3843−3849.

(13) Hancu, I. M.; Curto, A. G.; Castro-López, M.; Kuttge, M.; van Hulst, N. F. *Nano Lett.* **2014**, *14*, 166−171.

(14) Coenen, T.; Arango, F. B.; Koenderink, A. F.; Polman, A. *Nat. Commun.* **2014**, *5*, 3250.

(15) Panaro, S.; Nazir, A.; Liberale, C.; Das, G.; Wang, H.; De Angelis, F.; Zaccaria, R. P.; Di Fabrizio, E.; Toma, A. *ACS Photonics* **2014**, *1*, 310−314.

(16) Pan, D.; Wei, H.; Jia, Z. L.; Xu, H. X. *Sci. Rep.* **2014**, *4*, 4993 DOI: 10.1038/srep04993.

(17) López-Tejeira, F.; Rodrigo, S. G.; Martín-Moreno, L.; García-Vidal, F. J.; Devaux, E.; Ebbesen, T. W.; Krenn, J. R.; Radko, I. P.; Bozhevolnyi, S. I.; González, M. U.; Weeber, J. C.; Dereux, A. *Nat. Phys.* **2007**, *3*, 324−328.

(18) Chen, J. J.; Li, Z.; Yue, S.; Gong, Q. H. *Appl. Phys. Lett.* **2010**, *97*, 041113.

(19) Baron, A.; Devaux, E.; Rodier, J.-C.; Hugonin, J.-P; Rousseau, E.; Genet, C.; Ebbesen, T. W.; Lalanne, P. *Nano Lett.* **2011**, *11*, 4207−4212.

(20) Liu, J. S. Q.; Pala, R. A.; Afshinmanesh, F.; Cai, W. S.; Brongersma, M. L. *Nat.Commun.* **2011**, *2*, 525.

(21) Liu, Y.; Palomba, S.; Park, Y.; Zentgraf, T.; Yin, X.; Zhang, X. *Nano Lett.* **2012**, *12*, 4853−4858.

(22) Rodríguez-Fortuño, F. J.; Marino, G.; Ginzburg, P.; O'Connor, D.; Martínez, A.; Wurtz, G. A.; Zayats, A. V. *Science* **2013**, *340*, 328−330.

(23) Lin, J.; Mueller, J. P. B; Wang, Q.; Yuan, G.; Antoniou, N.; Yuan, X.-C.; Capasso, F. *Science* **2013**, *340*, 331−334.

(24) Liao, H. M.; Li, Z.; Chen, J. J.; Zhang, X.; Yue, S.; Gong, Q. H. *Sci. Rep.* **2013**, *3*, 1918 DOI: 10.1038/srep01918.

(25) Lalanne, P.; Hugonin, J. P.; Rodier, J. C. *Phys. Rev. Lett.* **2005**, *95*, 263902.

(26) Lalanne, P.; Hugonin, J. P.; Rodier, J. C. *J. Opt. Soc. Am. A* **2006**, *23*, 1608−1615.

(27) Raghunathan, S. B.; Gan, C. H.; van Dijk, T.; Kim, B. E.; Schouten, H. F.; Ubachs, W.; Lalanne, P.; Visser, T. D. *Opt. Express* **2012**, *20*, 15326−15335.

(28) Raghunathan, S. B.; Schouten, H. F.; Ubachs, W.; Kim, B. E.; Gan, C. H.; Visser, T. D. *Phys. Rev. Lett.* **2013**, *111*, 153901.

(29) Johnson, P. B.; Christy, R. W. *Phys. Rev. B* **1972**, *6*, 4370−4379.

(30) Snyder, A. W.; Love, J. D. *Optical Waveguide Theory*; Chapman and Hall: New York, 1983.

(31) Lalanne, P.; Hugonin, J. P.; Liu, H. T.; Wang, B. *Surf. Sci. Rep.* **2009**, *64*, 453−469.

(32) Nagpal, P.; Lindquist, N. C.; Oh, S.-H.; Norris, D. J. *Science* **2009**, *325*, 594−597.